CrossMark

Case Study on the γ-algorithm: Possible Tests from the Luminosity versus Displacement Correlation of High Mass X-Ray Binaries

Zhao-Yu Zuo and Huan Zhang

Ministry of Education Key Laboratory for Nonequilibrium Synthesis and Modulation of Condensed Matter, School of Physics, Xi'an Jiaotong University, Xi'an 710049, China; zuozyu@xjtu.edu.cn

Abstract

Using the apparent correlation of luminosity (L_X) versus displacement (R) of high mass X-ray binaries (HMXBs), we aim to constrain the common envelope (CE) mechanism, which is vital in the formation and evolution of compact binaries. We find that under the assumption of the γ-algorithm, the apparent correlation can also be reconstructed generally within a reasonable range of key parameters adopted, though the population of HMXBs is distinct with that in the canonical α_{CE}-formalism. We compare the spatial distribution of HMXBs under the two CE mechanisms, and suggest the difference in L_X versus R distribution may provide an additional clue for the study of the CE phase and to discriminate between CE models.

Key words: (stars:) binaries (including multiple): close – galaxies: starburst – stars: evolution – X-rays: binaries

1. Introduction

Common envelope (CE) evolution is considered a vital phase in close binary stars (Paczyński 1976). Beginning when the envelope of a star expands and overflows its Roche lobe (RL), a CE may form due to piles up of material transferred too high to be accreted by the companion star. The companion then starts to in-spiral through the CE. Orbital energy and angular momentum of the companion are then transferred to the envelope, leading to orbital decay and possibly the ejection of the CE. This may result in a stellar merger if ejection fails, or, if the pair survives, to the emergence of a binary with a closer orbit. The CE evolution is of great importance to explain the formation of diverse compact binaries and transients.

Despite this, little is known about the physics of CE evolution (see Ivanova et al. 2013, for reviews). The manner by which the envelope is removed remains extremely elusive. Many effects have been made using three-dimensional hydrodynamic simulations of CEs (e.g., Rasio & Livio 1996; Sandquist et al. 1998, 2000; Fryxell et al. 2000; O'Shea et al. 2005; Fryer et al. 2006; Passy et al. 2012; Ricker & Taam 2012; Ivanova & Nandez 2016; Nandez & Ivanova 2016; Sand et al. 2020), however due to a complex mix of physical processes involved in CEs which operate over a large dynamic range of scales, little is yet known about the physical details on CEs, such as hydrodynamics, turbulence, convection, accretion, radiation, self-gravity, nuclear burning, ionization/recombination, magnetism, jets, etc. (Passy et al. 2012; Ricker & Taam 2012; Ivanova et al. 2015; Soker 2015; Kuruwita et al. 2016; Ohlmann et al. 2016; Sabach et al. 2017; Chamandy et al. 2018; Glanz & Perets 2018; Grichener et al. 2018; Ivanova 2018; Kashi & Soker 2018; Soker et al. 2018). In order to use in population

synthesis studies, simplified and parameterized recipes are usually adopted to deal with the parameters of the pre- and post-CE orbit (Tutukov & Yungelson 1979). Two approaches are very popular, i.e., the energy budget approach (e.g., the α_{CE}-formalism, van den Heuvel 1976; Webbink 1984) and the angular momentum budget approach (the γ-algorithm, Nelemans et al. 2000; Nelemans & Tout 2005). However both the approaches can hardly explain the overall populations of post-CE binaries (PCEBs) or single stars observed, such as extreme horizontal branch stars (Han et al. 2002, 2003; Han 2008), white dwarf-main sequence (WD-MS, Politano & Weiler 2006, 2007; Davis et al. 2010, see also references therein), and low-mass X-ray binaries (LMXBs, Podsiadlowski et al. 2003), etc. New approaches such as the enthalpy prescription (Ivanova & Chaichenets 2011) and the grazing envelope evolution prescription (Soker 2015) are also proposed in recent years to account for the CE evolution. The recipe for the CE is still an open question to debate even up to today.

High mass X-ray binaries (HMXBs) are also good examples to investigate CEs. Binaries with tight initial orbits are subject to mergers due to CEs, but this would allow the binary to survive the supernova (SN) kick, resulting in luminous HMXBs. Typically, an HMXB may form after a dynamically stable or unstable mass transfer from the more massive primary to the secondary (Van Bever & Vanbeveren 2000; Tauris & van den Heuvel 2006; Linden et al. 2010). If mass transfer is dynamically unstable, a CE would occur, which may significantly shrink the binary orbit, resulting in binaries consisting of the primary's core and the secondary if survived. At the next stage, the primary's core would collapse to become a compact star, i.e., neutron star (NS) or black hole (BH). If the NS/BH could accrete from the

Table 1
Model Parameters

Model	G10	G11	G12	G13	G14/K110	G15	G16	G17	G18	K50	K190	K265
γ	1.0	1.1	1.2	1.3	1.4	1.5	1.6	1.7	1.8	1.4	1.4	1.4
σ_{kick}	110	110	110	110	110	110	110	110	110	50	190	265

Note. Here γ is the efficiency of the orbital angular momentum used to eject the CE, σ_{kick} is the dispersion of kick velocity in units of km s^{-1}.

secondary by capturing the stellar wind or Roche lobe overflow (RLOF), an HMXB may be born. Under some circumstances, the current system may also trigger a (second) CE, during which the envelope of the secondary could be peeled, resulting in an HMXB with a Wolf–Rayet (WR) companion. So the CE phase, by affecting the binary orbit, governs the evolution of an HMXB. The specific statistical characteristics exhibited by HMXBs as a population may therefore serve as a key to study the CE interaction.

Observationally, HMXB populations do have their unique statistical characteristics (for catalogs, see Liu et al. 2005, 2006). The X-ray luminosity function (XLF) of HMXBs is found to follow a single smooth power law form in the range of $\sim 10^{35}$–10^{40} erg s^{-1} (slope $\sim$1.6, Mineo et al. 2012, see also Grimm et al. 2003). The spatial displacements of HMXBs are also unique (i.e., L_X versus R distribution, Kaaret et al. 2004): (1) X-ray sources gather around the star clusters generally; (2) brighter sources are relatively closer to the clusters; and (3) luminous sources with $L_X > 10^{38}$ erg s^{-1} are found likely absent at relatively large displacements (i.e., larger than $\sim$200 pc). These studies are based on data from Chandra of X-ray sources and/or NICMOS onboard Hubble Space Telescope of star clusters.

Theoretical modelings regarding the effect of CE on HMXB populations have already been carried out. It is found that the efficiency parameter (i.e., α_{CE}) of CE, by controlling the orbit of binary, influences not merely the products of the population (i.e., HMXB XLF, Zuo et al. 2014), but also their kinetic motion, therefore the spatial offsets, showing as distinct L_X versus R distribution (Zuo & Li 2010, 2014b). Modeling of these statistics therefore gives a good constraint on the value of α_{CE} (Zuo & Li 2014b; Zuo et al. 2014). It seems that, under the assumption of the γ-algorithm, the HMXB XLF can also be well constructed to compare with the observation, but the detailed components are different (i.e., from XLF modelings, Zuo & Li 2014a, see Figure 3 therein). The spatial distribution and kinetics of HMXBs, which are of great importance to compare directly with the observation, however is still lacking.

In this paper, we applied an evolutionary population synthesis (EPS) technique which is most up-to-dated to simulate the spatial distribution of HMXBs under the assumption of the γ-algorithm. We considered different choices of the value of γ and the dispersion of kick velocity σ_{kick} (see Table 1 in Section 2), which are key parameters that affect HMXBs and their motion significantly. The objective of this

work is to check if the L_X versus R distribution in Kaaret et al. (2004) could be reconstructed within the typical value of γ. The spatial statistics of simulated HMXBs are also more feasible-to-check with high-resolution X-ray and optical observations in the future, which may largely help understand the evolution of CE and discriminate between CE models.

The organization of this paper is as follows. The EPS method and the basic assumptions for X-ray binaries (XRBs) are described in Section 2. The results are presented in Section 3, as well as discussions. The conclusions are drawn in Section 4.
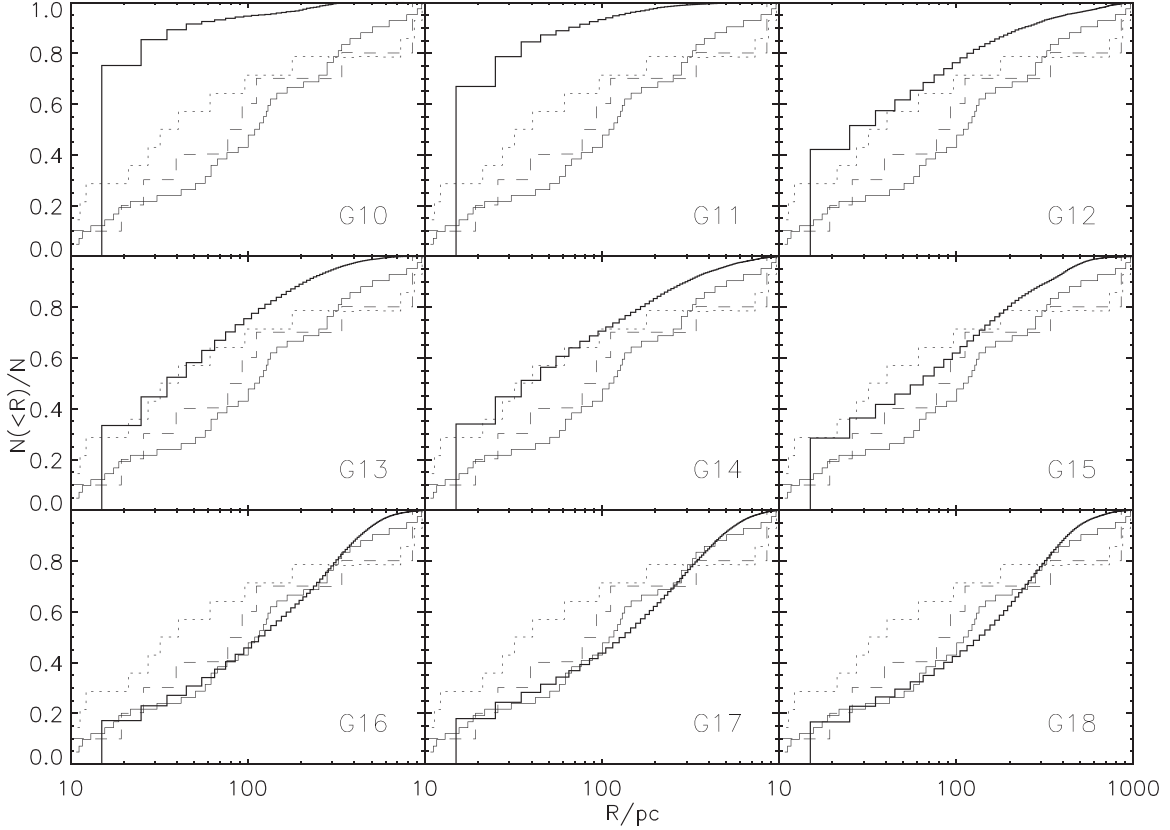
2. Model Description

2.1. Basic Assumptions and Binary Evolution

We use the recently updated EPS code (see Zuo et al. 2014, for details), which is originally designed by Hurley et al. (2000, 2002), to simulate the evolution of HMXBs,. The updates include several folds, such as prescriptions on compact object masses (i.e., the rapid SN mechanism, Fryer et al. 2012, see also Belczynski et al. 2012), massive stellar winds (Vink et al. 2001, also see Belczynski et al. 2010), fallback BH formations (Fryer & Kalogera 2001) and electron capture SN (i.e., ECS, Podsiadlowski et al. 2004) NSs. Furthermore, we update the criteria for CE occurrence as described in the text below.

To model the HMXB populations, a sample of 8×10^6 primordial binaries are evolved in each simulation. All stars are assumed to be born in binaries, in which a circular orbit is assumed. The initial parameters in the EPS computations are chosen the same as that in Hurley et al. (2002), and described as follows: (1) for primaries, the mass M_1 follows the initial mass function presented by Kroupa (2001, slope index -1.3 in 0.08–0.5 $M_\odot$, and -2.3 in 0.5–80.0 $M_\odot$); (2) the distribution of mass ratio is adopted constant, i.e., $n(q) = 1$, in which $0 < q = M_2/M_1 \leqslant 1$, to give the secondary mass M_2; (3) the distribution of binary separations is constant in $\ln a$, with a in range of 3–10^4 $R_\odot$. The values of other parameters are the same as these in Zuo et al. (2014) if not mentioned otherwise. The rate of star formation (SF) is fixed constant for 20 Myr in order to be in line with Kaaret et al. (2004). We briefly describe the input parameters, as well as the basic assumptions in the control model (i.e., model G14/K110, see Table 1) below.

(1) *CE evolution* In the case of unstable mass transfer, a CE would form to swallow up the binary. To enter the CE, the mass ratio $q \equiv M_{donor}/M_{accretor}$ is crucial. There exists a critical value

Figure 1. Normalized cumulative distribution of source displacements (thick-solid line) for models G10-G18 (see Table 1), respectively. The thin-solid, dashed and dotted lines represent the observed cumulative distributions in galaxies M82, NGC 5253 and NGC 1569 (i.e., Figure 2, Kaaret et al. 2004), respectively.

for q, denoted as q_c. If q exceed q_c, mass transfer is dynamically unstable, then a CE forms. The ratio q_c depends on the evolutionary state of the donor star when RLOF occurs (Hjellming & Webbink 1987; Podsiadlowski et al. 2002; Chen & Han 2008; Pavlovskii et al. 2017; Shao & Li 2021). In the current study, we use an updated q_c presented by Shao & Li (2014, model II, which is an intermediate between Models I and III with 50% of the transferred mass accreted) for CE initiated by Hertzsprung gap donors. For giants, we follow the recipes presented by Hurley et al. (2002, see Equation (57) and descriptions therein).

For the CE mechanism, we consider the γ-algorithm, which is an alternative recipe to depict the CE interaction besides the canonical α_{CE}-formalism. It is introduced when studying some double WD binaries, the α_{CE}-formalism (Webbink 1984, here α_{CE} is the efficiency of the released orbital energy used for ejections of the CE) needs α_{CE} physically unrealistic high (or even negative), beyond the range of the reasonable value expected. Instead Nelemans et al. (2000) parameterized the CE interaction in terms of γ, that's to say, the efficiency of the
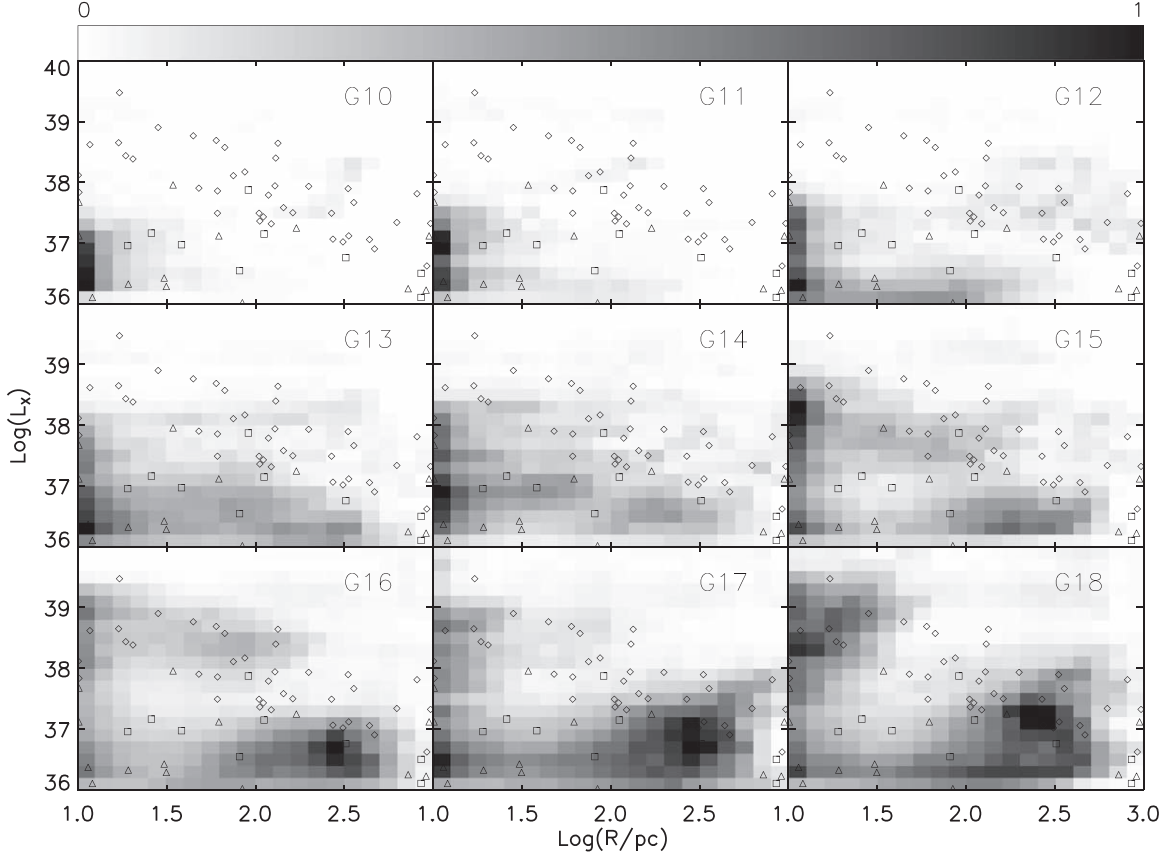
orbital angular momentum used to eject the CE, as follows,

$$\frac{\triangle J_b}{J_b} = \gamma \frac{M_{env}}{M_1 + M_2} \tag{1}$$

where J_b represents the total angular momentum of the binary, and $\triangle J_b$ the change of J_b during the CE phase. After the CE, the orbital separation of the pre-CE, a_i, becomes a_f which is given by the following equation,

$$\frac{a_f}{a_i} = \left(\frac{M_1}{M_c}\right)^2 \left(\frac{M_c + M_2}{M_1 + M_2}\right)\left[1 - \gamma\left(\frac{M_{env}}{M_1 + M_2}\right)\right]^2 \tag{2}$$

where M_1, M_2, M_c and M_{env} are the masses of the primary, the secondary, the helium-core and envelope of the giant, respectively. The formula above may produce not only the distribution of double WDs well, but also several other PCEBs hosting WDs (Nelemans & Tout 2005). Moreover, the value of γ is in a fairly narrow range (i.e., ~1.5–1.75), which is regarded as a significant advantage of the γ-algorithm.

For the CE evolution, we assume a global value of 1.4 for γ in the control model (model G14/K110, see Table 1).

Figure 2. Distribution of L_X vs. R for models G10-G18 (see Table 1), respectively. The symbols represent sources in Kaaret et al. (2004, Figure 3, diamonds: M82; squares: NGC 5253 and triangles: NGC 1569) sample, shown for comparison.

Table 2
2D K-S Test for Each Model, Along with the Fractions of HMXBs Whose Progenitors Experienced at least One CE Phase (f_{CE} in Percent)
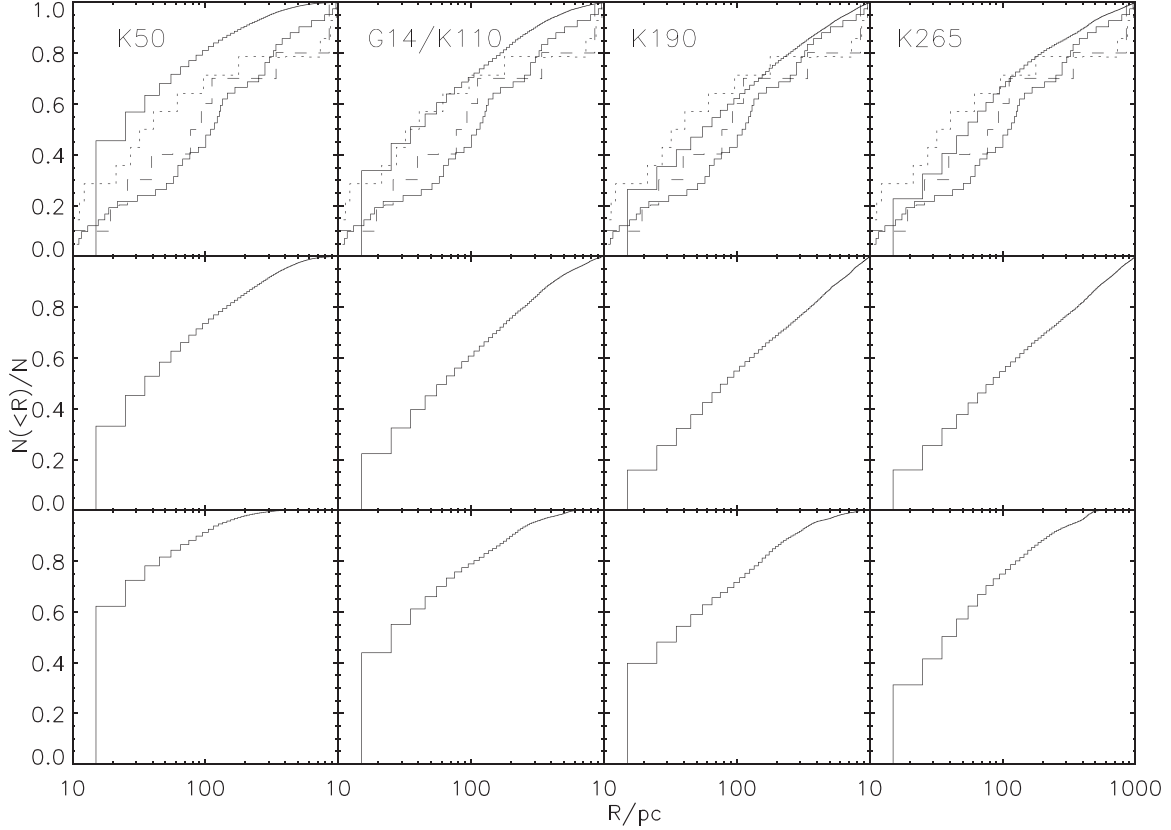
Model	G10	G11	G12	G13	G14/K110	G15
p-value	8×10^{-7}	2×10^{-5}	0.11	0.4	0.6	0.63
f_{CE}	26	34	43	53	61	68

Model	G16	G17	G18	K50	K190	K265
p-value	0.9	0.77	0.77	0.03	0.9	0.72
f_{CE}	73	80	88	64	57	54

Moreover, in order to measure the effect of γ, it was given different values in several cases of the first and second CE episodes, but no significant changes were found in our basic conclusions. To fully explore the parameter space, we also vary the γ value from 1.0 to 1.8. These models are denoted as G10, G11, G12, G13, G15, G16, G17, and G18 where the number following each code corresponds the γ value for the CE episodes, respectively.

(2) *SN kicks* The natal SN kick imparted onto the newborn NS/BH is still very uncertain (Zuo & Li 2014b). For NS natal kicks ($v_{k,NS}$), a Maxwellian distribution is assumed, as follows,

$$P(v_{k,NS}) = \sqrt{\frac{2}{\pi}} \frac{v_k^2}{\sigma_{kick}^3} \exp\left(-\frac{v_{k,NS}^2}{2\sigma_{kick}^2}\right); \qquad (3)$$

where σ_{kick} is the dispersion of kick velocity. It is assigned $110 \, \mathrm{km \, s^{-1}}$ in the basic model (i.e., model G14/K110, see Table 1), and 50 (model K50), 190 (model K190, Hansen & Phinney 1997), 265 km s^{-1} (model K265, Hobbs et al. 2005) to measure its effect. For natal kick of BH ($v_{k,BH}$), we adopt the fallback prescription given by Fryer et al. (2012, also see Dominik et al. 2012). The BH kicks decrease linearly with increasing material-fallback fraction f_{back}, that is to say, by a factor of $(1 - f_{back})$. In addition, it is assumed that BHs formed with little fallback ($M_{fb} < 0.2 \, M_\odot$) receive full natal kicks. And if BHs form silently via direct collapse (i.e., $f_{back} = 1$), we assume no natal kick. We assume no natal kick for ECS NSs as well (Podsiadlowski et al. 2004).

Figure 3. Similar to Figure 1 but for ALL-XRBs (top row), NS-XRBs (middle row) and BH-XRBs (bottom row) in models K50, G14/K110, K190, and K265 from left to right, respectively.

2.2. Binary Motion

The system velocity (v_{sys}) for binary stars is computed as follows (see Hurley et al. 2002, for the detail),

$$v_{sys} = \frac{M_1'}{M_b'}v_{k,NS/BH} - \frac{\triangle M_1 M_2}{M_b' M_b}v,\qquad(4)$$

where $M_1' = M_1 - \Delta M_1$ is the current mass of the primary after the lost of ΔM_1 mass during the SN. $M_b = M_1 + M_2$ is the total masses of the system before the SN explosion, and $M_b' = M_b - \Delta M_1$ after the SN explosion. V is the relative orbital velocity of the stars (i.e., Equation (A1), Hurley et al. 2002). Obviously, the orbital velocity of the system is closely linked to the system velocity v_{sys}.
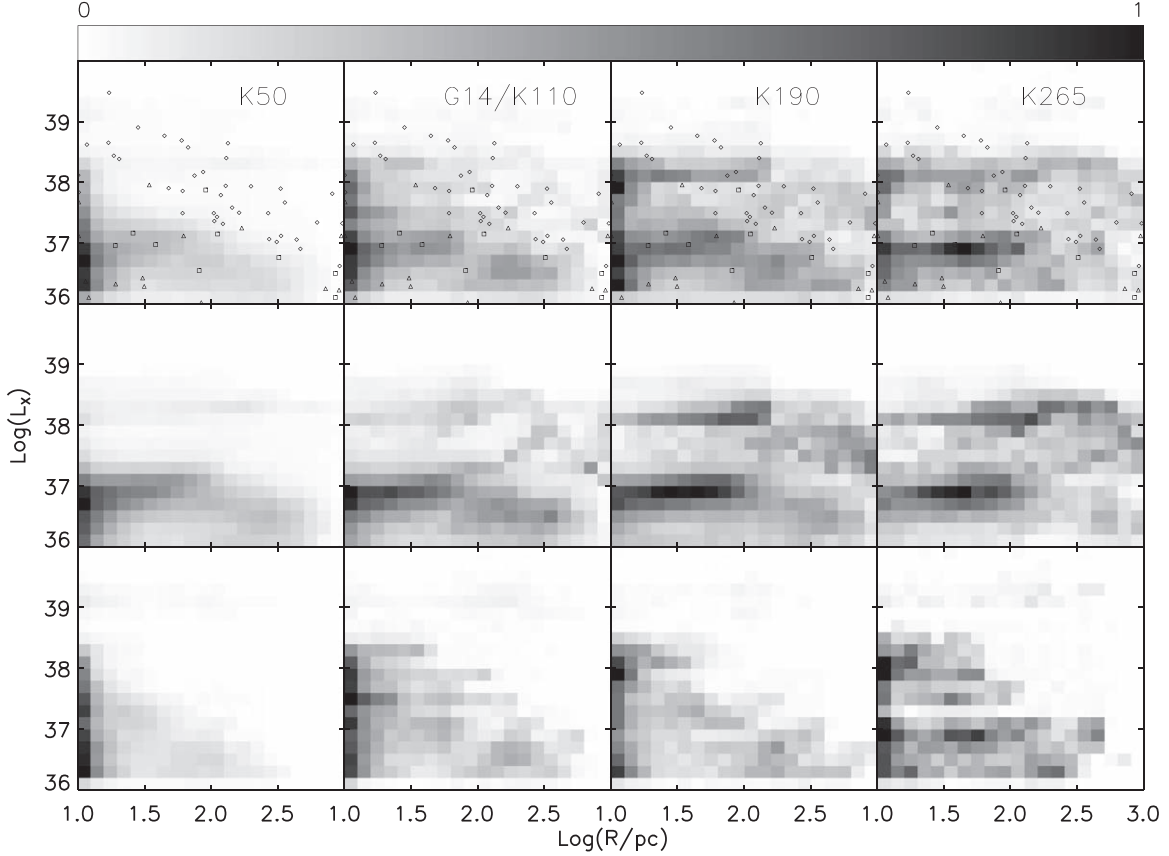
To calculate the trajectories of HMXBs, we adopt the same method as in Zuo & Li (2010, see Section 2.1.2 therein for details). Considering that the mass of the star cluster is concentrated in the center, a spherical potential is assumed, described in cylindrical coordinate system (r, ϕ, z), as follows,

$$\Phi(r, z) = \frac{-GM}{\sqrt{r^2 + z^2} + h},\qquad(5)$$

where M is the total mass of stars within the half light radius, h. The basic parameters are as follows: (1) $h = 3$ pc and $M = 1.0 \times 10^6 M_\odot$ (Ho & Filippenko 1996a, 1996b); (2) We assume stars are born uniformly throughout the cluster; (3) For the initial velocity, the direction of a star is chosen randomly. We integrate the motion equations (see Equations 19(a) and (b) in Paczyński 1990) with a fourth-order Runge–Kutta method, and then collect parameters of current binaries if it becomes XRBs. The HMXB distribution can then be determined by two space coordinates (i.e., r and z) because of symmetries of the potential. The spatial offsets of HMXBs are then calculated as $R = ((r\cos\varphi)^2 + z^2)^{1/2}$, i.e., projected on the $\phi = 0$ plane, with φ distributed uniformly in [0, 2π]. In the simulation, we set the integral accuracy to be 10^{-6}, which is governed by the energy integral.

2.3. XRB Assumption

We adopt the same procedure as in Zuo et al. (2014, see Section 2.2 therein for more details) to compute the X-ray luminosity. In this work, we ignore LMXBs (with donor mass $<2\,M_\odot$) and Be-XRBs since they are expected minor in young

Figure 4. Similar to Figure 2 but for ALL-XRBs (top row), NS-XRBs (middle row) and BH-XRBs (bottom row) in models K50, G14/K110, K190, and K265 from left to right, respectively.

populations (Zuo & Li 2014b). We adopt the classical formula of Bondi & Hoyle (1944, see Equation (6) in Hurley et al. 2002) for wind-powered systems. For disk-fed sources, we use Equation (36) in Lasota (2001) to discriminate persistents and transients. The X-ray luminosity is then computed according to:

$$L_{X,0.5-8\,\text{keV}}$$
$$= \begin{cases} \eta_{bol}\eta_{out}L_{Edd} & \text{transients,} \\ \eta_{bol}\min(L_{bol}, \eta_{Edd}L_{Edd}) & \text{persistents.} \end{cases} \quad (6)$$
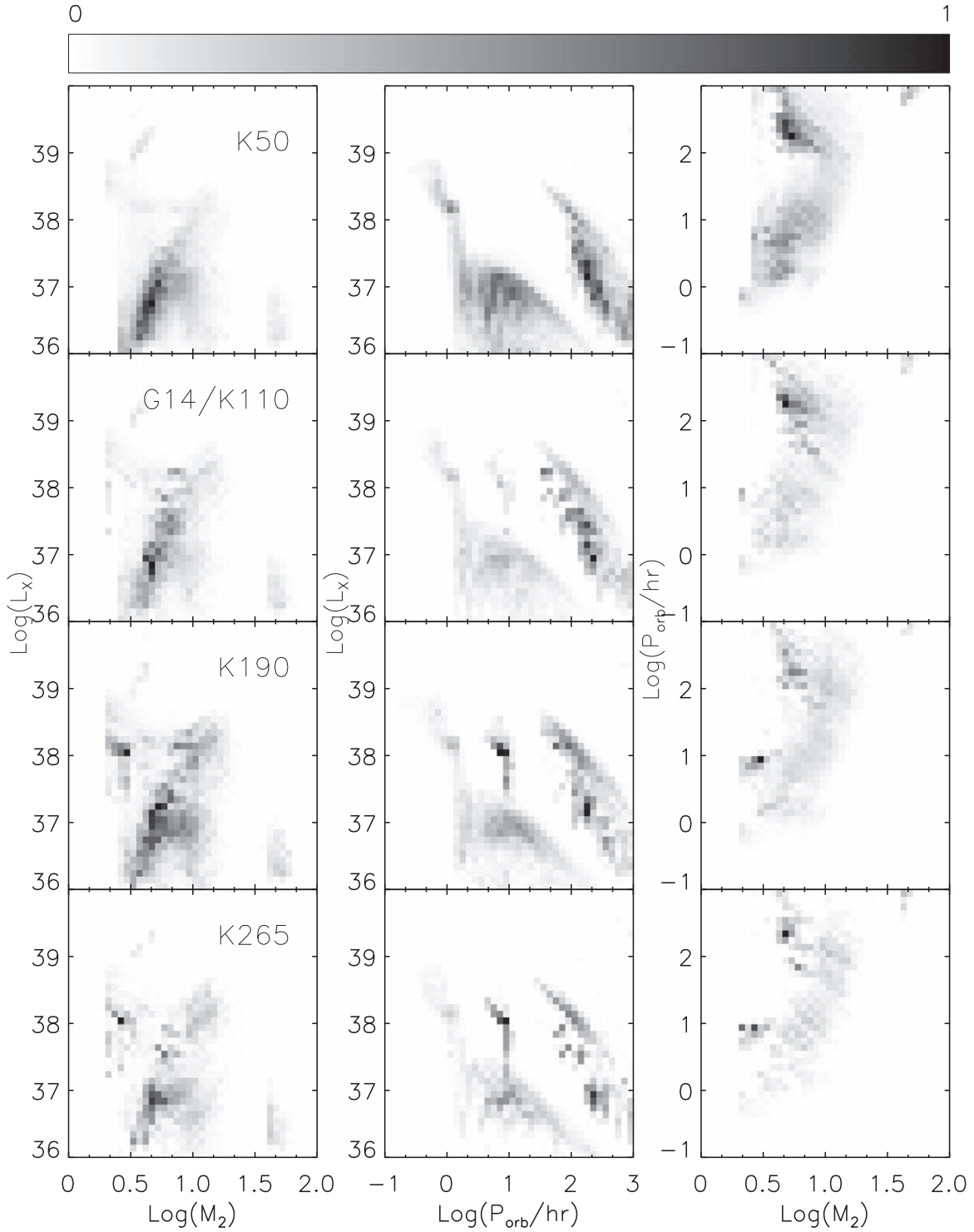
The parameters are explained as follows: (1) L_{bol} is the bolometric luminosity, $\simeq 0.1\dot{M}_{acc}c^2$, where $\dot{M}_{acc}$ is the average mass accretion rate and c light speed; (2) η_{bol} is the bolometric correction factor, adopted as 0.1 for NS-XRBs and 0.2 for BH-XRBs, respectively; (3) η_{Edd} represents the maximum super-Eddington accretion rate allowed, adopted as 5 and 100 for NS and BH XRBs, respectively (Zuo et al. 2014). (4) the critical Eddington luminosity $L_{Edd} \simeq 4\pi GM_{acc}m_p c/\sigma_T = 1.3 \times 10^{38}m_{acc}$ erg s^{-1}, where m_{acc} is the mass of accretor M_{acc} in solar mass, m_p the proton mass, and σ_T the Thomson cross section; (5) the luminosity of transients in outbursts is chosen as a fraction (i.e., η_{out}) of L_{Edd}, with η_{out}

adopted as 1 and 0.1 for NS(BH) transients with orbital period longer and shorter than 1 day(10 h), respectively (Chen et al. 1997; Garcia et al. 2003; Belczynski et al. 2008).
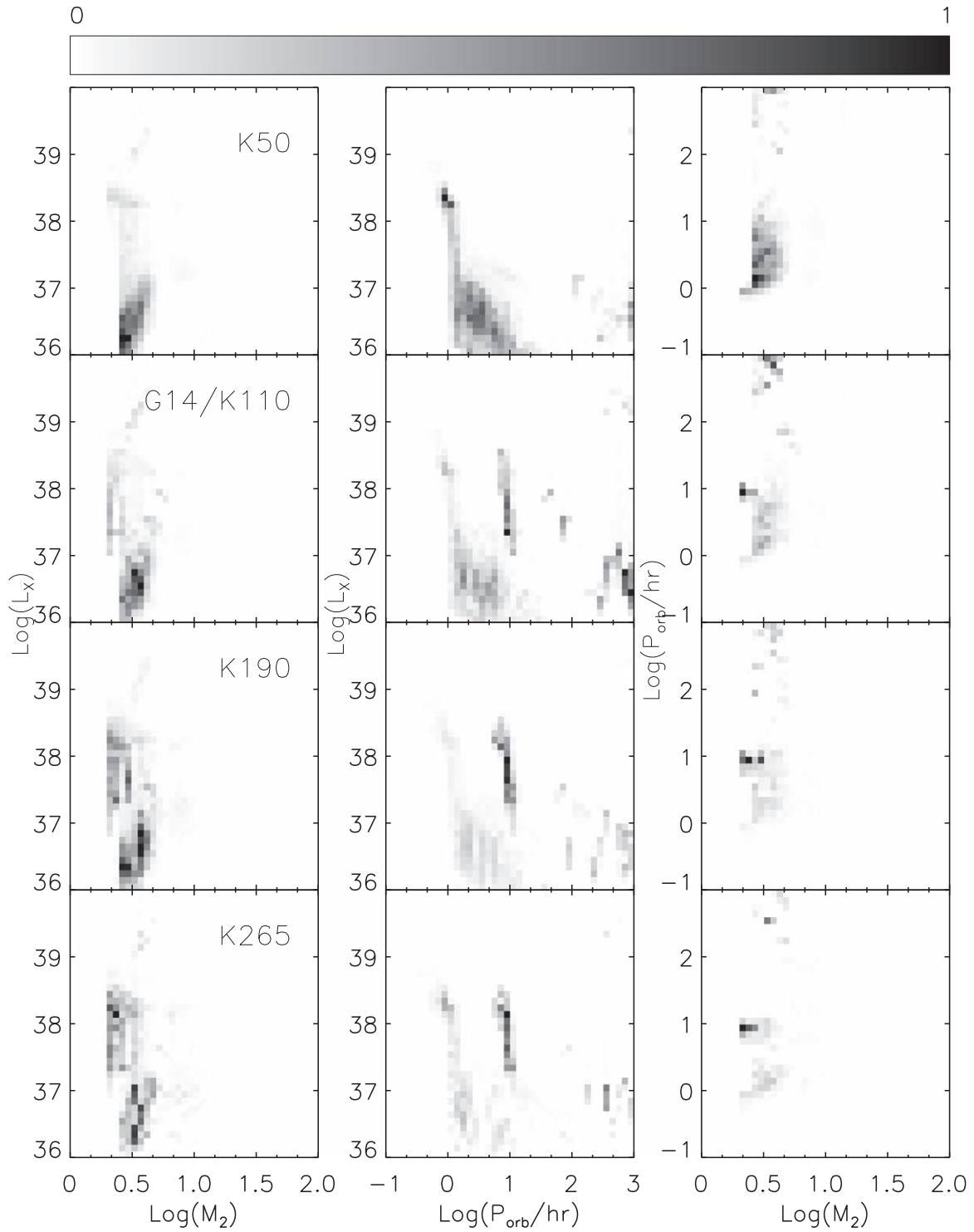
3. Results

In order to compare with the statistics (i.e., L_X versus R distribution) derived by Kaaret et al. (2004), several models were constructed, as listed in Table 1. In our control model (i.e., model G14/K110), a global value of $\gamma = 1.4$ is adopted and $\sigma_{kick} = 110$ km s^{-1}. In other models, only one parameter is changed each time to observe its effect. To evaluate our results, a two-dimensional Kolmogorov–Smirnov (2D K-S, Fasano & Franceschini 1987) test is performed through cumulative curves, and we observe the distributions in the L_X versus R plane for further check, as already done in Zuo & Li (2014b, for more details).

Figures 1 and 2 show the cumulative displacement distribution and the normalized distribution (color bar: occurrence possibility) of L_X versus R of XRBs in models G10–G18, respectively. Only sources within 10–1000 pc of a star cluster are taken into account. To construct the cumulative

Figure 5. Distributions of L_X–M_2 (left), L_X–P_{orb} (middle), and P_{orb}–M_2 (right) of XRBs with offsets R in 10–100 pc for models K50, G14/K110, K190, and K265 from top to bottom, respectively.

Figure 6. Same as in Figure 5 but for XRBs with offsets R in 100–1000 pc (regions C).

Table 3
Detailed Source Type of XRBs in Region A ($L_X > 10^{38}$ erg s^{-1}, Offsets R in 10–100 pc)

Model	BH Percent	$\frac{N(>10^{38}\text{ erg s}^{-1})}{N(>10^{36}\text{ erg s}^{-1})}$	$\frac{\text{BHMS}}{\text{BH}}$	$\frac{\text{BHHeMS}}{\text{BH}}$	$\frac{\text{NSMS}}{\text{NS}}$	$\frac{\text{NSHeMS}}{\text{NS}}$
K50	58	9	11	89	1	99
G14/K110	65	15	8	92	5	95
K190	52	21	6	94	15	85
K265	50	20	4	96	12	88

Note. Here BH percent is the percentage of BH-XRBs in region A, $\frac{N(>10^{38}\text{ erg s}^{-1})}{N(>10^{36}\text{ erg s}^{-1})}$ is the percentage of sources with $L_X > 10^{38}$ erg s^{-1} in small offsets region (i.e., $R \in$ [10–100] pc). "NS(BH)MS" and "NS(BH)HeMS" represent NS(BH)-XRBs with MS donors and NS(BH)-XRBs with HeMS donors, respectively.

Table 4
Detailed Source Type of XRBs in Region B ($10^{36} < L_X < 10^{38}$ erg s^{-1}, Offsets R in 10–100 pc)

Model	BH Percent	$\frac{N(10^{36} < L_X < 10^{38}\text{ erg s}^{-1})}{N(>10^{36}\text{ erg s}^{-1})}$	$\frac{\text{BHMS}}{\text{BH}}$	$\frac{\text{BHHeMS}}{\text{BH}}$	$\frac{\text{NSMS}}{\text{NS}}$	$\frac{\text{NSHeMS}}{\text{NS}}$
K50	47	91	8	92	5	95
G14/K110	60	85	8	92	5	95
K190	50	79	8	92	11	89
K265	51	80	10	90	14	86

Note. Here $\frac{N(10^{36} < L_X < 10^{38}\text{ erg s}^{-1})}{N(>10^{36}\text{ erg s}^{-1})}$ is the percentage of sources with $10^{36} < L_X < 10^{38}$ erg s^{-1} in small offsets region (i.e., $R \in$ [10–100] pc). See also Table 3 for other details.

Table 5
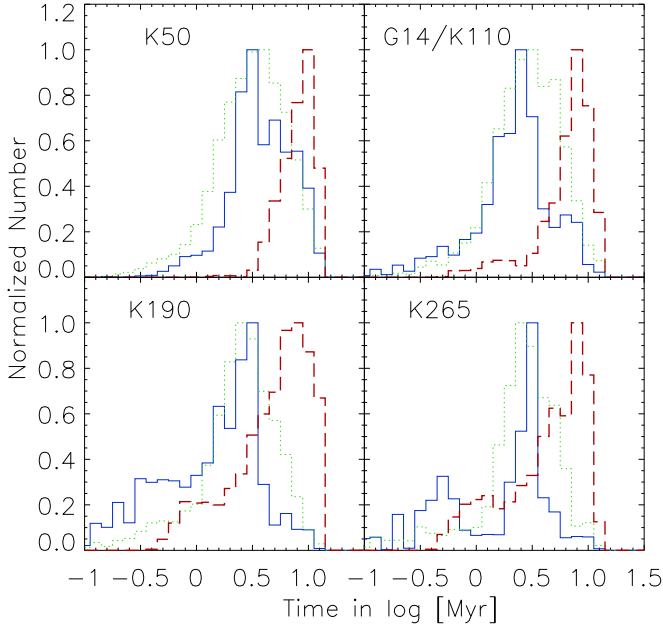Detailed Source Type of XRBs in Region C ($L_X > 10^{36}$ erg s^{-1}, Offsets R in 100–1000 pc)

Model	BH Percent	$\frac{N(>10^{38}\text{ erg s}^{-1})}{N(>10^{36}\text{ erg s}^{-1})}$	$\frac{\text{BHMS}}{\text{BH}}$	$\frac{\text{BHHeMS}}{\text{BH}}$	$\frac{\text{NSMS}}{\text{NS}}$	$\frac{\text{NSHeMS}}{\text{NS}}$
K50	19	10	4	96	1	99
G14/K110	38	12	3	97	5	95
K190	27	27	3	97	13	87
K265	27	28	2	98	10	90

Note. $\frac{N(>10^{38}\text{ erg s}^{-1})}{N(>10^{36}\text{ erg s}^{-1})}$ is the percentage of sources with $L_X > 10^{38}$ erg s^{-1} in region C. See also Table 3 for other details.

displacement distribution of XRBs (Figure 1), only sources in 10^{36} and 10^{38} erg s^{-1} are selected in order to compare with Kaaret et al. (2004). One can see that models with the value of $\gamma \sim 1.3$–1.5 can compare generally with the observational statistics simultaneously in both distributions, while other models likely fail, in particular for models with $\gamma < \sim1.1$ (i.e., models G10 and G11, the values of p less than 10^{-5}, see Table 2, along with the fractions of HMXBs whose progenitors experienced at least one CE phase, i.e., f_{CE} in percent.). We note the larger the value of γ is, the higher f_{CE} would be. When compared with the results obtained by HMXB XLF modelings (Zuo & Li 2014a, i.e., $\gamma < \sim1.5$), the two results are basically consistent.

With the range of γ values narrowed down, we also change the dispersion of kick velocity σ_{kick} (see Table 1), which may affect HMXBs and their motion significantly. The value of γ is fixed as 1.4 in this case for simplicity. Similarly, the

distributions of cumulative displacements (similar to Figure 1) and L_X versus R (similar to Figure 2) of XRBs are presented in Figures 3 and 4, respectively. It is shown that models with $\sigma_{kick} > \sim100$ km s^{-1} (i.e., models G14/K110, K190 and K265, possibility ~0.6–0.9, see Table 2) can in general be compared with the observation while model K50 (with too weak natal kicks, possibility $\sim10^{-2}$) clearly fail. We note that these results are in agreement with our previous findings by simulating HMXB XLF (Zuo et al. 2014) and HMXB kinetics (Zuo 2015). In addition, When compared with Zuo & Li (2014b, i.e., α_{CE}-formalism), the general feature of L_X versus R correlation is comparable, however the distribution of BH XRBs seems different. A significant proportion of BH XRBs can move to much farther places (even to region C, $R \in$ [100, 1000] pc) in the case of γ-algorithm, while it appears mainly at small-offsets ($R \in$ [10, 100] pc) in the α_{CE}-formalism (Zuo & Li 2014b, see Figure 4 for comparison), though

Figure 7. Distributions of delay time from SN explosion to the turning-on of X-rays in region A (solid line), region B (dotted line), and region C (dashed line) for models K50, G14/K110, K190, and K265, respectively.

spreading from high luminosities ($L_X > 10^{38}\,\mathrm{erg\,s^{-1}}$, known as regions A), to low luminosities ($10^{36} < L_X < 10^{38}\,\mathrm{erg\,s^{-1}}$, known as regions B).
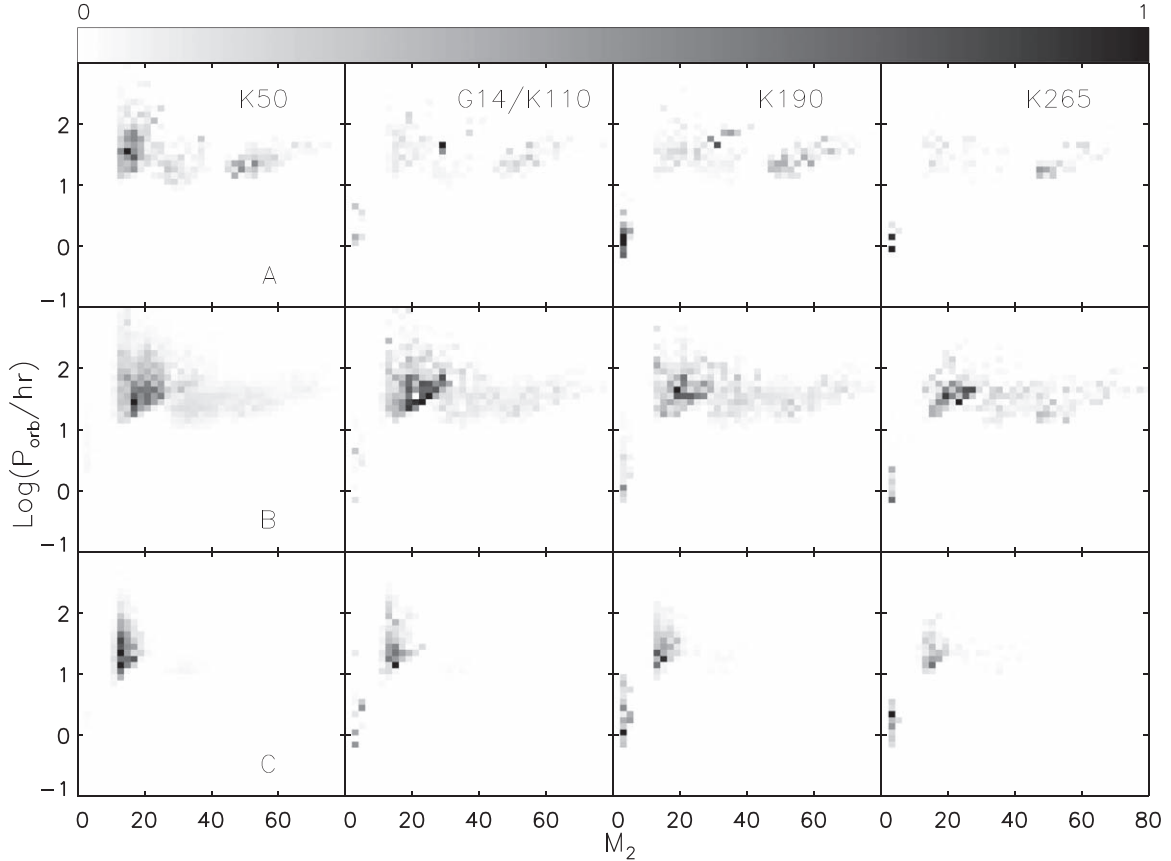
The properties of XRBs in each region are essential to compare between models and with observations. In Figures 5 and 6, the distributions among orbital period P_{orb}, current mass M_2, and X-ray luminosity L_X are explored for models K50, G14/K110, K190 and K265 with offsets R in 10–100 pc (regions A and regions B) and 100–1000 pc (regions C), respectively. We also present the corresponding source types in Tables 3–5.

Figure 5 shows that, XRBs in regions A have short orbits (P_{orb} about a few hours for NS XRBs, and up to days for BHs). The donors are mainly helium main-sequence (HeMS) stars with masses about a few to $10\,M_\odot$. The binary velocities are relatively low, mainly $\sim30\,\mathrm{km\,s^{-1}}$, and few up to $\sim100\,\mathrm{km\,s^{-1}}$ for NS XRBs. Seeing from Figure 7 that their evolutionary timescales (generally $<\sim3$ Myr) are also relative short, they are hardly able to travel too far, even ~100 pc. The XRBs in regions B appear diversities. One subgroup is very similar to those in regions A, that is to say, similar binary velocities, similar HeMS donors, but with slightly longer orbital periods, i.e., hours to days for NS XRBs, and up to tens of days for BH XRBs. The other subgroup is dominated by low-speed (with velocities less than $\sim30\,\mathrm{km\,s^{-1}}$) BH-XRBs, powered by stellar winds from massive (~30–$60\,M_\odot$) MS donors, mainly in low luminosities ($\sim10^{36}$–$10^{37}\,\mathrm{erg\,s^{-1}}$). They have much wider orbits (periods about several tens of days). In

Figure 6, we see that the XRBs in regions C mainly have low-mass ($<\sim4\,M_\odot$) HeMS donors, with orbital periods mainly about a few hours to days. Their typical velocities are ~30–$100\,\mathrm{km\,s^{-1}}$ for BH XRBs, and ~100–$200\,\mathrm{km\,s^{-1}}$ for NS XRBs, which is larger than those in small offsets (regions A and B). In view of that their evolutionary timescales in regions C (mainly ~10 Myr, see Figure 7) is also relatively longer than that in regions A and B, they could be able to move much farther than other sources. It is clear that besides the velocities of binary system after SN, the spatial offsets of XRBs also depend on the delay time from SN to the onset of X-rays, as shown in Figure 7 the normalized distributions in different regions (solid line: regions A; dotted line: regions B; dashed line: regions C). We note that XRBs in regions C clearly have relatively much longer evolutionary timescale than those in regions A and B. XRBs in regions A could reach the shortest evolutionary timescales, though it is generally similar to sources in regions B overall.

We note the population of XRBs under the γ-algorithm is distinct with that in Zuo & Li (2014b, i.e., the α_{CE}-formalism). The most remarkable difference is that, even for BH HMXBs, they may still get a large displacement, as far as even hundreds of pc. It seems that there are much more low mass (about several solar mass) HeMS XRBs when compared with that in Zuo & Li (2014b, i.e., the α_{CE}-formalism), especially for BH XRBs at relatively large displacements. We suggest the difference of XRB population in different offset regions may provide an additional clue to distinguish CE models. In comparison with the statistics of current observations, the amount of current observed HMXBs with WR donors seems small, i.e., only one WR XRB, i.e., Cyg X-3, in the Galaxy (van Kerkwijk et al. 1992), and several in the extragalactic regions (Esposito et al. 2015, see their Table 6) confirmed. The mass of the WR donors is massive (Esposito et al. 2015, see their Table 6), which is suspected to suffer from the selection effect of observations. It was thought, in predicting the existence of WR XRBs, that any helium star with mass $\gtrsim3$–$4\,M_\odot$ could be identified as a WR star. However, recent studies, either from terms of absolute luminosity or in binaries, suggest that the identification mass for WR stars needs to be adjusted to $\gtrsim10(\pm2)M_\odot$ (Crowther 2007; Sander et al. 2012). In this aspect, we suggest the spatial distribution of HMXBs, as well as their detailed properties, are no doubt helpful for us to better study the CE phase and distinguish CE models. Future high-resolution optical and X-ray observations, as well as high-precision astrometry measurements of HMXBs in nearby star-forming galaxies, are still needed.

In addition, the difference of binary velocities between regions is still tightly related to the orbital period $P_{\mathrm{orb,SN}}$ (or orbital velocity), as well as the companion mass $M_{2,\mathrm{SN}}$ during the SN explosion (see Equation (4)), as already noted in Zuo & Li (2010). Generally the source with a long period (hence small orbital velocity) and a massive companion leads to a small

Figure 8. Distribution of $P_{orb,SN}$–$M_{2,SN}$ in regions A (top), B (middle), and C (bottom) for models K50, G14/K110, K190, and K265 from left to right, respectively.

system velocity, therefore small offsets from the birthplace. It can be seen clearly in Figure 8, that is to say, the distribution of $P_{orb,SN}$–$M_{2,SN}$ in each region. The long period, massive donor pre-SN systems in regions A and B are much more than in region C, which may explain why they are mainly low speed sources generally.
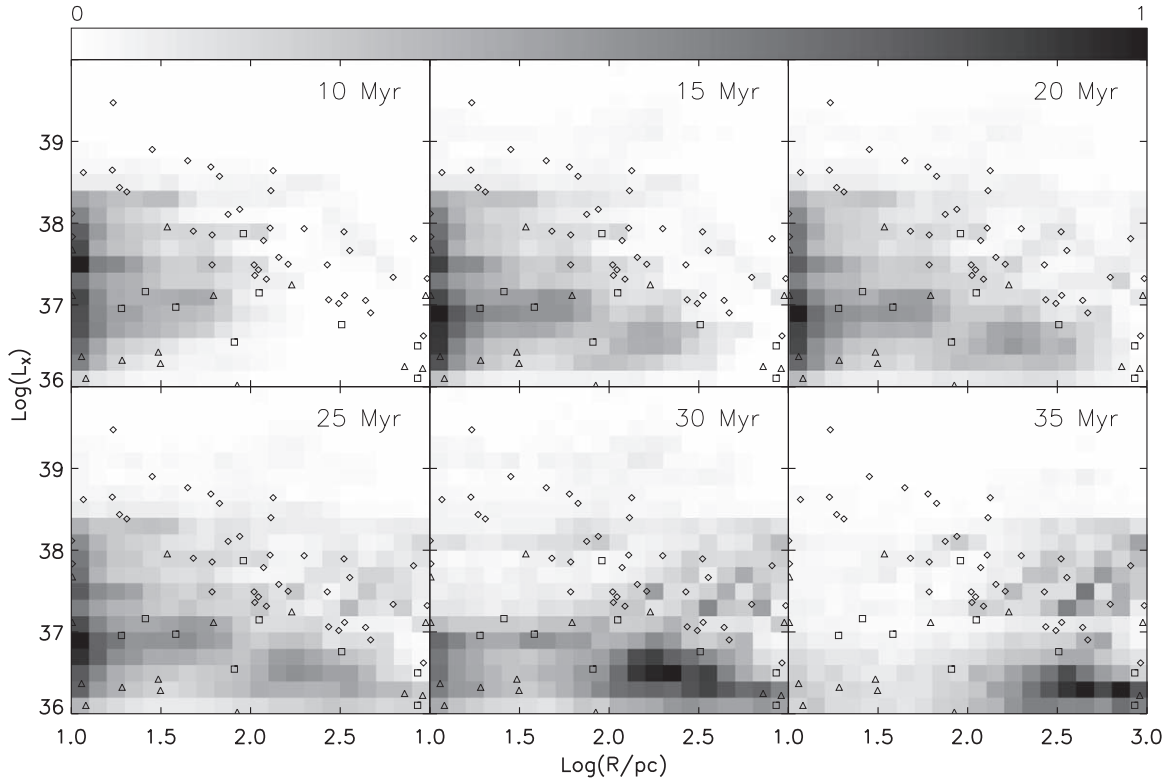
The prevalence and wide spread of BH-He XRBs is significantly different from that in Zuo & Li (2014b, i.e., the α_{CE}-formalism), which is still caused by CE prescriptions adopted, as already noted in Zuo & Li (2014a). The typical progenitors of BH-He HMXBs usually have massive primaries in the mass range of $\sim$35–80 $M_{\odot}$, less massive ($\sim$10–30 $M_{\odot}$) secondaries, and their orbits range from tens to hundreds $R_{\odot}$. So the α_{CE}-formalism always result in binary mergers because of the large envelope binding energy installed. But the γ-algorithm acts in a different way. The orbit during the CE phase is determined only by two parameters, $q = M_{donor}/M_{accretor}$ (the mass ratio) and $u = M_c/M_{donor}$ (the core mass fraction). As deduced from Equation (6) and seen clearly from Figure 3 in Nelemans & Tout (2005), the binary orbit not only can shrink, but also may expand, which not only prevent from mergers of binary, but also delay the onset of the X-rays significantly, as

illustrated clearly by comparing Figure 7 in this study with Figure 7 in Zuo & Li (2014a, i.e., the α_{CE}-formalism), also see Figure 7 in Zuo & Li (2014a). This is also why these binaries have much longer time to move in the cluster potential, resulting in farther spatial offsets.

In Figure 9, we present the evolution of L_X versus R distribution for model G14/K110. The times were set from 10 to 35 Myr in a 5 Myr interval after the SF started. We note the L_X versus R correlation is also gradually built up and may disappear for individual cluster, which is similar to the case in the α_{CE}-formalism (i.e., Figure 10, Zuo & Li 2014b).

4. Conclusions

By integrating the trajectories of binary systems within the cluster potential, this study modeled the L_X versus R distribution of HMXB population under the assumption of the γ-algorithm. We find that under the typical value of γ, the L_X versus R distribution could also be reconstructed generally to compare with the observation, though the population of HMXBs in this case is distinct with that in the canonical α_{CE}-formalism (Zuo & Li 2014b). It seems that there are much more low mass (about several solar mass) HeMS HMXBs

Figure 9. The evolution of the L_X vs. R distribution with time (from 10 to 35 in 5 Myr interval since the beginning of SF) for model G14/K110.

under the assumption of the γ-algorithm, which are however not found yet, though it might be due to the selection effect of observations, that is to say, only massive WR ($\gtrsim 10(\pm 2)M_\odot$, Crowther 2007; Sander et al. 2012) could be easily identified. Especially, BH HMXB with low mass HeMS companion are found at relatively large displacements which are nearly absent in the case of the α_{CE}-formalism. We suggest that these differences may provide additional evidence for the study of the CE phase and to distinguish CE models. We stress that through this case study, it is clearly verified that the CE mechanisms, through governing the binary orbit, take a critical part in the kinetic motion, and hence the spatial offsets of the sources. The distinct distribution of L_X versus R on the contrary can make further constraints (Zuo & Li 2014b) or possible tests on CE. We also present the detailed properties and kinetics of the model-predicted present-day HMXBs under the assumption of the γ-algorithm, which may be further testified by future high-resolution optical and X-ray observations of HMXBs in nearby star-forming galaxies.

Acknowledgments

ORCID iDs

Zhao-Yu Zuo ⓘ https://orcid.org/0000-0001-6693-586X

References

Belczynski, K., Bulik, T., Ruiter, A., et al. 2010, ApJ, 714, 1217
Belczynski, K., Kalogera, V., Rasio, F. A., et al. 2008, ApJS, 174, 223
Belczynski, K., Wiktorowicz, G., Fryer, C., Holz, D., & Kalogera, V. 2012, ApJ, 757, 91
Bondi, H., & Hoyle, F. 1944, MNRAS, 104, 273
Chamandy, L., Frank, A., Blackman, E., et al. 2018, MNRAS, 480, 1898
Chen, W., Shrader, C. R., & Livio, M. 1997, ApJ, 491, 312
Chen, X., & Han, Z. 2008, MNRAS, 387, 1416
Crowther, P. A. 2007, ARA&A, 45, 177
Davis, P. J., Kolb, U., & Willems, B. 2010, MNRAS, 403, 179
Dominik, M., Belczynski, K., Fryer, C., et al. 2012, ApJ, 759, 52
Esposito, P., Israel, G. L., Milisavljevic, D., et al. 2015, MNRAS, 482, 1112
Fasano, G., & Franceschini, A. 1987, MNRAS, 225, 155
Fryer, C. L., Belczynski, K., Wiktorowicz, G., et al. 2012, ApJ, 749, 91
Fryer, C. L., & Kalogera, V. 2001, ApJ, 554, 548
Fryer, C. L., Rockefeller, G., & Warren, M. S. 2006, ApJ, 643, 292
Fryxell, B., Olson, K., Ricker, P., et al. 2000, ApJS, 131, 273
Garcia, M. R., Miller, J. M., McClintock, J. E., King, A. R., & Orosz, J. 2003, ApJ, 591, 388
Glanz, H., & Perets, H. B. 2018, MNRAS, 478, L12
Grichener, A., Sabach, E., & Soker, N. 2018, MNRAS, 478, 1818
Grimm, H.-J., Gilfanov, M., & Sunyaev, R. 2003, MNRAS, 339, 793

Han, Z. 2008, A&A, 484, L31
Han, Z., Podsiadlowski, P., Maxted, P. F. L., & Marsh, T. R. 2003, MNRAS, 341, 669
Han, Z., Podsiadlowski, P., Maxted, P. F. L., Marsh, T. R., & Ivanova, N. 2002, MNRAS, 336, 449
Hansen, B., & Phinney, E. 1997, MNRAS, 291, 569
Hjellming, M. S., & Webbink, R. F. 1987, ApJ, 318, 794
Ho, L. C., & Filippenko, A. V. 1996a, ApJL, 466, L83
Ho, L. C., & Filippenko, A. V. 1996b, ApJ, 472, 600
Hobbs, G., Lorimer, D. R., Lyne, A. G., & Kramer, M. 2005, MNRAS, 360, 963
Hurley, J. R., Pols, O. R., & Tout, C. A. 2000, MNRAS, 315, 543
Hurley, J. R., Tout, C. A., & Pols, O. R. 2002, MNRAS, 329, 897
Ivanova, N. 2018, ApJL, 858, L24
Ivanova, N., & Chaichenets, S. 2011, ApJL, 731, 36
Ivanova, N., Justham, S., & Podsiadlowski, P. 2015, MNRAS, 447, 2181
Ivanova, N., & Nandez, J. L. A. 2016, MNRAS, 462, 3621
Ivanova, N., Justham, S., Chen, X., et al. 2013, A&ARv, 21, 59
Kaaret, P., Alonso-Herrero, A., Gallagher, J. S., et al. 2004, MNRAS, 348, L28
Kashi, A., & Soker, N. 2018, MNRAS, 480, 3195
Kroupa, P. 2001, MNRAS, 322, 231
Kuruwita, R. L., Staff, J., & De Marco, O. 2016, MNRAS, 461, 486
Lasota, J. P. 2001, NewAR, 45, 449
Linden, T., kalogera, V., Sepinsky, J. F., et al. 2010, ApJ, 725, 1984
Liu, Q. Z., van Paradijs, J., & van den Heuvel, E. P. J. 2005, A&A, 442, 1135
Liu, Q. Z., van Paradijs, J., & van den Heuvel, E. P. J. 2006, A&A, 455, 1165
Mineo, S., Gilfanov, M., & Sunyaev, R. 2012, MNRAS, 419, 2095
Nandez, J. L. A., & Ivanova, N. 2016, MNRAS, 460, 3992
Nelemans, G., & Tout, C. A. 2005, MNRAS, 356, 753
Nelemans, G., Verbunt, F., Yungelson, L. R., & Portegies Zwart, S. F. 2000, A&A, 360, 1011
O'Shea, B. W., Nagamine, K., Springel, V., Hernquist, L., & Norman, M. L. 2005, ApJS, 160, 1
Ohlmann, S. T., Röpke, F. K., Pakmor, R., & Springel, V. 2016, ApJL, 816, L9
Paczyński, B. 1990, ApJ, 348, 485
Paczyński, P. 1976, in Proc. IAU Symp. 73, Structure and Evolution of Close Binary Systems, ed. P. Eggleton, S. Mitton, & J. Whelan (Dordrecht: Reidel), 75
Passy, J.-C., De Marco, O., Fryer, C., et al. 2012, ApJ, 744, 52

Pavlovskii, K., Ivanova, N., Belczynski, K., & Van, K. X. 2017, MNRAS, 465, 2092
Podsiadlowski, P., Langer, N., Poelarends, A. J. T., et al. 2004, ApJ, 612, 1044
Podsiadlowski, P., Rappaport, S., & Pfahl, E. D. 2002, ApJ, 565, 1107
Podsiadlowski, P., Rappaport, S. A., & Han, Z. 2003, MNRAS, 341, 385
Politano, M., & Weiler, M. 2006, ApJL, 641, L1373
Politano, M., & Weiler, M. 2007, ApJ, 665, 663
Rasio, F., & Livio, M. 1996, ApJ, 471, 366
Ricker, P. M., & Taam, R. E. 2012, ApJ, 746, 74
Sabach, E., Hillel, S., Schreier, R., & Soker, N. 2017, MNRAS, 472, 4361
Sand, C., Ohlmann, S. T., Schneider, F. R. N., Pakmor, R., & Röpke, F. K. 2020, A&A, 644, 60
Sander, A., Hamann, W.-R., & Todt, H. 2012, A&A, 540, 144
Sandquist, E. L., Taam, R. E., & Burkert, A. 2000, ApJ, 533, 984
Sandquist, E. L., Taam, R. E., Chen, X., Bodenheimer, P., & Burkert, A. 1998, ApJ, 500, 909
Shao, Y., & Li, X. D. 2014, ApJ, 796, 37
Shao, Y., & Li, X. D. 2021, ApJ, 920, 81
Soker, N. 2015, ApJ, 800, 114
Soker, N., Grichener, A., & Sabach, E. 2018, ApJL, 863, L14
Tauris, T. M., & van den Heuvel, E. P. J. 2006, in Compact Stellar X-ray Sources, ed. W. Lewin & M. van der Klis (Cambridge: Cambridge Univ. Press), 623
Tutukov, A., & Yungelson, L. 1979, in IAU Symp. 83, Mass Loss and Evolution of O-Type Stars, ed. P. S. Conti & C. W. H. De Loore (Dordrecht: Reidel), 401
Van Bever, J., & Vanbeveren, D. 2000, A&A, 358, 462
van den Heuvel, E. P. J. 1976, in IAU Symp. 73, Structure and Evolution of Close Binary Systems, ed. P. Eggleton, S. Mitton, & J. Whelan (Dordrecht: Reidel), 35
van Kerkwijk, M. H., Charles, P., Geballe, T., et al. 1992, Natur, 355, 703
Vink, J. S., de Koter, A., & Lamers, H. J. G. L. M. 2001, A&A, 369, 574
Webbink, R. F. 1984, ApJ, 277, 355
Zuo, Z. Y. 2015, A&A, 573, A58
Zuo, Z. Y., & Li, X. D. 2010, MNRAS, 405, 2768
Zuo, Z. Y., & Li, X. D. 2014a, ApJ, 797, 45
Zuo, Z. Y., & Li, X. D. 2014b, MNRAS, 442, 1980
Zuo, Z. Y., Li, X. D., & Gu, Q. S. 2014, MNRAS, 437, 1187